CARBON 52 (2013) 83–89

Available at www.sciencedirect.com

SciVerse ScienceDirect

journal homepage: www.elsevier.com/locate/carbon

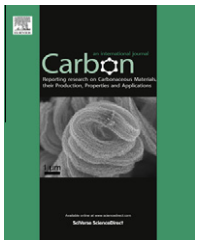

Formation of high-quality quasi-free-standing bilayer graphene on SiC(0001) by oxygen intercalation upon annealing in air

Myriano H. Oliveira Jr. [a], *Timo Schumann* [a], *Felix Fromm* [b], *Roland Koch* [b], *Markus Ostler* [b], *Manfred Ramsteiner* [a], *Thomas Seyller* [b], *Joao Marcelo J. Lopes* [a,*], *Henning Riechert* [a]

[a] *Paul-Drude-Institut für Festkörperelektronik, Hausvogteiplatz 5-7, 10117 Berlin, Germany*
[b] *Lehrstuhl für Technische Physik, Universität Erlangen-Nürnberg, Erwin-Rommel-Str. 1, 91058 Erlangen, Germany*

ARTICLE INFO

Article history:
Received 18 July 2012
Accepted 6 September 2012
Available online 15 September 2012

ABSTRACT

We report on the conversion of epitaxial monolayer graphene on SiC(0001) into decoupled bilayer graphene by performing an annealing step in air. We prove by Raman scattering and photoemission experiments that it has structural and electronic properties that characterize its quasi-free-standing nature. The $(6\sqrt{3}\times 6\sqrt{3})R30^\circ$ buffer layer underneath the monolayer graphene loses its covalent bonding to the substrate and is converted into a graphene layer due to the oxidation of the SiC surface. The oxygen reacts with the SiC surface without inducing defects in the topmost carbon layers. The high-quality bilayer graphene obtained after air annealing is *p*-doped and homogeneous over a large area.

1. Introduction

Graphene is a two-dimensional material that has been shown to exhibit very unique and interesting physical properties [1–3]. Due to some of these properties, such as very high carrier mobility [4] and ballistic transport at room temperature [5], it has been considered to be a promising candidate for future applications in semiconductor technology.

Regarding its synthesis, growth of epitaxial graphene on the hexagonal surfaces of silicon carbide (SiC) by temperature-induced depletion of Si atoms appears to be a promising route. With this technique, it is possible to produce high-quality graphene on wafer-size areas [6,7] directly on an insulating substrate that is technologically compatible [5,8,9]. Despite these advantages, there are some factors that may limit the technological application of this material. Although it has been reported that graphene grown on the SiC(000−1) polar face behaves electronically very similar to free-standing graphene, offering for instance high charge carrier mobilities, a precise control over the number of grown layers is, however, difficult to be achieved [10–12]. The growth of an homogeneous monolayer graphene on the SiC(0001) face can be, in contrast, controllably achieved [6,13,14]. Nevertheless in this case the charge carrier mobility at room temperature is drastically reduced in comparison to that measured for free-standing graphene [6,15,16]. This is due to an interaction between the monolayer graphene and the substrate, which is mediated by a buffer layer (BL). This BL, also called zero-layer graphene, is a $(6\sqrt{3}\times 6\sqrt{3})R30^\circ$ carbon monolayer with an atomic arrangement similar to that of graphene [16,17]. The difference between this layer and a graphene one is that, instead of being composed of only sp^2 hybridized atoms, the BL has about 30% of its carbon atoms covalently bonded to the Si atoms of the SiC interface [17] probably including a significant degree of rehybridization to a more sp^3-like configuration. Due to this strong coupling with the substrate, the

* *Corresponding author:* Fax: +49 30 20377 201.
E-mail address: lopes@pdi-berlin.de (J.M.J. Lopes).
0008-6223/$ - see front matter
http://dx.doi.org/10.1016/j.carbon.2012.09.008

BL does not exhibit graphene-like π bands and is, consequently, electronically inactive [16–18].

By thermally treating a BL sample in a high-purity hydrogen atmosphere, Riedl et al. [19] showed that it is possible to detach the BL from the SiC substrate. This occurs because the hydrogen diffuses underneath the BL and breaks the covalent bonding between its $(6\sqrt{3}\times 6\sqrt{3})R30^\circ$ structure and the substrate. The H atoms bond to the topmost Si atoms and passivate the SiC surface. Consequently, the BL becomes completely sp^2 hybridized and develops the structural and electronic properties of monolayer graphene. The transport properties of this material, called by the authors quasi-free-standing graphene [19], were recently investigated by Speck et al. [20] and Waldmann et al. [9]. They showed that the H intercalated quasi-free-standing monolayer graphene has charge carrier mobility almost independent on the temperature. At room temperature this mobility is about 3.5 times larger than that of conventional epitaxial monolayer graphene on top of the BL. The production of quasi-free-standing bilayer graphene by intercalating H underneath epitaxial monolayer graphene has also been achieved [19,21–23]. The latter is of extreme importance for electronic applications, since bilayer graphene has an electric field tunable band gap [3,24–26].

Decoupling a BL and/or an epitaxial monolayer graphene by intercalation of other elements such as fluorine [27,28], silicon [29], gold [30,31], germanium [32], lithium [33], as well as oxygen [34,35], has also been reported. F intercalation to generate monolayer graphene has shown to be partial and not homogeneous [27,28]. In addition, Wong et al. [28] has shown, by using X-ray photoemission spectroscopy (XPS), that a fraction of the intercalated F atoms establishes covalent bonds with the graphene layer. Interestingly, production of bilayer graphene could not be achieved using this element. The Si, Au, Ge, or Li intercalation is based on the deposition of an ultra-thin film of the desired element on top of a BL, or monolayer graphene, followed by their temperature-driven diffusion below the carbon layers [29–33]. The process requires careful control over the deposition and annealing parameters and it appears not to be straightforward to achieve a homogeneous intercalation. Intercalation of Si has been shown to not be able to generate quasi-free standing bilayer graphene over large areas [29]. Au intercalation induces defects and leads to the formation of Au clusters on top of the graphene layer [30,31]. Furthermore, the intercalated atoms have a non-negligible interaction with the graphene. In the case of Ge [32], the decoupling of the BL to generate a monolayer graphene has been demonstrated. However, there is no report on the generation of bilayer graphene. Virojanadara et al. [33] demonstrated that Li atoms are able to diffuse through the monolayer graphene and the BL and intercalate at the interface between the BL and the SiC substrate. However, the intercalation is not complete. As observed by XPS, the BL component on the C1S core level spectra does not vanish after the process, showing that a fraction of the BL is still covalently bonded to the SiC. Furthermore, no information about intercalation over large areas has been reported. The oxygen intercalation, on the other hand, is realized by employing thermal treatments in an O_2 atmosphere. The decoupling in this case is associated with the formation of a thin oxide layer underneath the BL [34,35]. Oida et al. [34] investigated this process by using photoemission experiments. However, no information was given about the intercalation uniformity and structural quality of the resulting graphene layers. In a later study Ostler et al. [35] showed that decoupling the BL by oxidation of the SiC interface introduces a large amount of defects in the graphene, promoted by an oxygen etching of the carbon layer.

In this contribution, we report on the decoupling of epitaxial monolayer graphene on SiC(0001) grown in an Ar atmosphere [6,36], *via* oxygen intercalation upon thermal annealing performed in air. This process allows the production of high-quality quasi-free-standing bilayer graphene. The changes promoted in the chemical bonding states within the material during annealing were investigated by XPS, which revealed the conversion of the BL into graphene as well as the oxidation of the SiC interface. The analysis of the structural properties, which was based on the atomic vibrational modes by Raman spectroscopy, showed the high structural quality of the resulting bilayer graphene as well as the intercalation uniformity over the entire sample area ($1\times 1\,cm^2$). The electronic band structure, investigated by angle resolved photoelectron spectroscopy (ARPES), confirms these results. The present method is a straightforward route to form large area and homogeneous bilayer graphene on SiC(0001), which is of major significance for future applications in graphene-based devices.

2. Experimental

Epitaxial monolayer graphene was grown on 6H-SiC(0001) substrates ($1\times 1\,cm^2$) cut from a nominally on-axis 2 inch *n*-type wafer polished on the (0001) face (epi-ready process by NovaSiC). The samples were chemically cleaned in n-butylacetate, acetone and methanol. The following processing steps, namely the H-etching and graphene growth, were both performed in a furnace equipped with an induction heating system. The H-etching treatment was carried out at 1400 °C for 15 min in a forming gas atmosphere (95 at.% Ar and 5 at.% H) of 900 mbar and a flow rate of 500 sccm. The epitaxial monolayer graphene was prepared at 1600 °C for 15 min in a 900 mbar Ar atmosphere also with a flow rate of 500 sccm.

Oxygen intercalation was accomplished by thermally treating the samples for 40 min at 600 °C in air with a preceding heating ramp of 50 °C/min.

Raman measurements were performed before and after oxygen intercalation with a spatial resolution of 1 μm using the 482.5 nm-line of a Kr^+ ion laser for excitation. The spatial resolution allowed performing measurements at the surface terraces (typically 5 μm wide, as determined by atomic force microscopy), without any contribution of the step edges. The absolute positions of the Raman peaks were calibrated using the emission lines of a Neon lamp. All Raman spectra shown in this paper correspond to the result obtained after the subtraction of the Raman signal of a bare SiC substrate from the original data.

XPS measurements were carried out with a Specs Phoibos 150 analyzer using a monochromated Al Kα X-ray source. Prior to the measurements, the samples were annealed at temperatures up to 400 °C for 20 min in ultra-high-vacuum (UHV) to remove contaminants from their surface.

ARPES was carried out using synchrotron radiation at the beamline UE56/L-PGM2 at BESSY II in Berlin, Germany. For angle and energy resolved detection of the photoelectrons, we employed a Specs Phoibos 100 analyzer in combination with a six axis liquid nitrogen cooled manipulator. The sample temperature during measurement is expected to be about 120 K. The resolution obtained was ~70 meV.

3. Results and discussion

Fig. 1a and b display the C1s core level spectra obtained by XPS measurements performed before and after thermal annealing in air at 600 °C for 40 min, respectively. The spectrum of the pristine monolayer graphene on SiC(0001) shows four components, one at 284.8 eV related to the carbon bonded within the graphene layer, the SiC bulk component at 283.9 eV, and the BL components S_1 (285.0 eV) and S_2 (285.7 eV). The lower energy component S_1 is due to the covalent bonds between the BL and the SiC surface, while S_2 is related to the sp^2 bonded carbon within the BL [17]. By using the ratio between the intensities of the overlayer and the SiC substrate components, the layer thickness was determined and corresponds to a monolayer graphene on top of a BL [37]. On the other hand, after thermal treatment in air, no BL-related components are observed in the C1s core level spectrum (Fig. 1b), which is now only composed of the graphene (at 284.4 eV) and bulk SiC (at 283.2 eV) components. Furthermore, the intensity of the graphene component increased after the annealing process and the thickness corresponds to bilayer graphene. These results show that the covalent bonds between the BL and the SiC were broken after thermal treatment and that the former was converted into a graphene layer.

The shift of 0.4 eV in binding energy between the graphene components of the C1s spectra corresponds to a difference in doping level between the pristine monolayer graphene (Fig. 1a) and the decoupled bilayer graphene obtained upon annealing in air (Fig. 1b). Also the SiC bulk component in the C1s (Fig. 1) and Si2p (Fig. 2) core level spectra shifts 0.7 eV towards lower binding energy. This reveals that the BL/SiC interfacial region is modified after annealing, causing a different band bending. The modification of the interface is confirmed by the presence of oxygen in the thermally treated sample. While the pristine monolayer graphene is oxygen-free (Fig. 2a), the Si2p core level spectrum reveals that the SiC is oxidized after annealing, showing two oxide components, Si^{+} and Si^{4+} (Fig. 2b), which are shifted with respect to the SiC bulk line by 0.48 and 2.0 eV, respectively. It is worth to notice that the lack of other components in the C1s core-level spectrum (Fig. 1b) shows that the oxygen does not interact covalently with the carbon layers. The analysis of the O1s spectral region (not shown) also reveals the oxygen-free nature of the pristine monolayer graphene as well as the oxygen incorporation after annealing in air. Measurements performed with different take-off angles (0° and 60°) confirm that the oxygen is indeed located at the bilayer graphene/SiC interface and not at the graphene surface. We can therefore

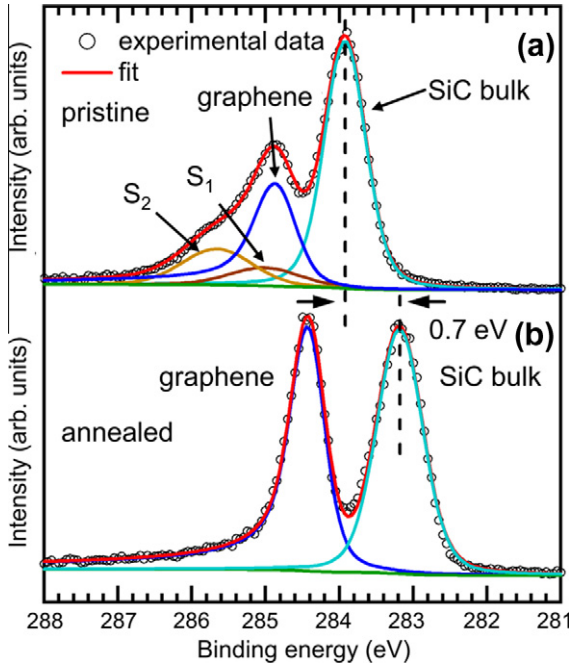

Fig. 1 – C1s core level spectra of (a) pristine monolayer graphene and (b) decoupled bilayer graphene after thermal treatment in air. The spectra were fitted with Voigt profiles for SiC bulk and BL components and a Doniach–Sunjic profile for the graphene components to account for the asymmetric line shape.

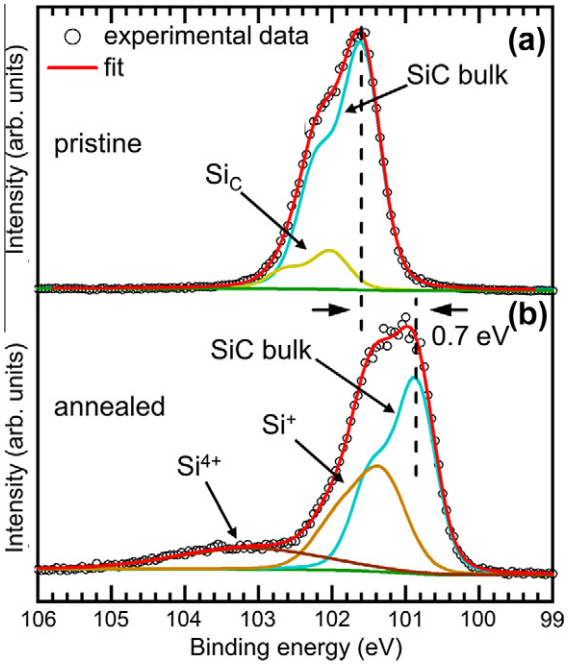

Fig. 2 – Si2p core level spectra of (a) pristine monolayer graphene and (b) decoupled bilayer graphene after thermal treatment in air. The spectra were fitted using Voigt doublets to account for the spin orbit splitting. The spectrum of the pristine monolayer graphene was fitted with two doublets, labeled SiC bulk and Si_C, corresponding to silicon in the SiC bulk and silicon at the SiC surface bonded to carbon within the buffer layer, respectively.

conclude that, during the air annealing, oxygen precursors (O_2 or H_2O) diffuse underneath the BL, break the covalent bonding of the BL with the SiC, and build up an oxide-terminated SiC surface. Such a process converts the system from monolayer graphene on BL to decoupled bilayer graphene.

Raman spectra of graphene samples obtained before and after the oxygen intercalation are displayed in Fig. 3a and b, respectively. Several measurements were performed over the entire surface area ($1 \times 1\ cm^2$), always on the terraces in order to avoid the contribution of the few-layer graphene (usually bi- or trilayer) existing at the step edges [38]. The Raman spectra of graphene show two main features, the *G* (~1580 cm^{-1}) and 2*D* (~2700 cm^{-1}) peaks. The former corresponds to the symmetric E_{2g} phonon at the Brillouin zone center [39] and the second to a second-order phonon scattering induced by a double-resonance process [40,41].

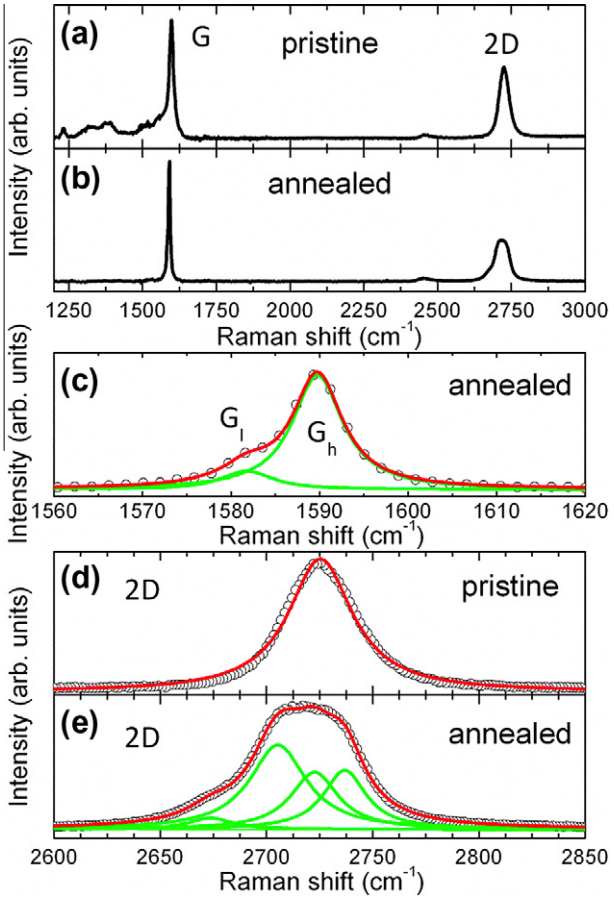

Fig. 3 – Raman spectra of: (a) pristine monolayer graphene and (b) quasi-free-standing bilayer graphene after thermal treatment in air. The *G* peak splitting in two components (c) for the decoupled bilayer graphene is fitted by two Lorentzians. The 2*D* peaks of the spectra in (a) and (b) are shown in detail in (d) and (e), respectively. The 2*D* peak of the pristine monolayer graphene (d) is fitted by one Lorentzian with 36 cm^{-1} of width. The 2*D* peak of the spectrum obtained after thermal treatment (e) has typical characteristics of free-standing bilayer graphene, and is fitted by four Lorentzians.

For the pristine monolayer graphene (Fig. 3a) the *G* peak position varies between 1593 and 1604 cm^{-1} [with a mean value of (1598 ± 4) cm^{-1}] for measurements performed on different surface regions. This variation of the *G* peak position is attributed to the existence of areas with different strain and charge carrier concentration [42–46]. Despite of having homogeneous morphology and being continuous over the whole substrate surface, it is known that epitaxial monolayer graphene can display substantial fluctuations in strain and charge carrier concentration [46,47]. Apart from this frequency variation, all spectra show the typical features of high-quality monolayer graphene on top of SiC, namely a narrow full width at half-maximum (FWHM) of (14 ± 1) cm^{-1} for the *G* peak, and a double-resonance peak (2*D*) at (2727 ± 10) cm^{-1} which can be well fitted by a single Lorentzian with FWHM of (36 ± 2) cm^{-1} (Fig. 3d). The estimated errors for the Raman parameters correspond to the standard deviation extracted from the distribution of peak positions. Based on the position of the *G* and 2*D* peaks [42–45], and using the Grüneisen parameters γ as determined by Zabel et al. [48] [$\gamma(G) = 1.8$ and $\gamma(2D) = 2.6$], a mean compressive strain of 0.2%, and a carrier density of $n = 3.7 \times 10^{12}\ cm^{-2}$, were extracted. Such values are in the range of those reported for epitaxial monolayer graphene on SiC(0001) [46].

The Raman spectra collected after oxygen intercalation show features of free-standing bilayer graphene. A closer look on the *G* band (Fig. 3c) reveals that its shape is asymmetric with a shoulder at lower wavenumbers. The splitting of the *G* line into two modes, named G_h and G_l (or G^+ and G^-, respectively), has been observed in gated [49,50] and asymmetrically-doped (due to adsorbates) bilayer graphene [51]. It has been shown that the induced dipole moment formed between the graphene layers breaks the inversion-symmetry [3,25,26,52] and, consequently, activates the antisymmetric mode E_u [49]. The mixing of the E_{2g} and E_u phonon modes is responsible for the *G* peak splitting [50,53] and is highly

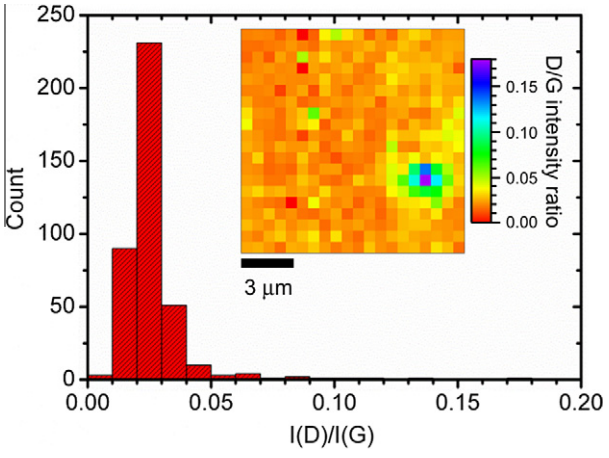

Fig. 4 – Histogram of *D*/*G* peaks intensity ratio [I(*D*)/I(*G*)] acquired from a Raman mapping (inset) taken from an area of 15 × 15 μm^2. The low intensity of the *D* peak and its uniformity over the mapped area confirms the high-quality and homogeneity of the quasi-free-standing bilayer graphene.

dependent on the difference in charge density between the bottom and top layers of graphene [49–51,53,54]. For the intercalated sample, the higher energy mode (G_h) is centered in the 1589–1593 cm^{-1} range, with a mean value of (1591 ± 1) cm^{-1}, while the lower energy mode (G_l) has its center in the range of 1581–1588 cm^{-1}, with mean value of (1584 ± 2) cm^{-1}. Each mode is fitted by a single Lorentzian with FWHM of 7 and 9 cm^{-1}, respectively. The reduction of the FWHM of the *G* peak after the intercalation, as well as the decreased variation in peak position, reflects the structural homogeneity of the bilayer graphene and shows that the intercalation is homogeneous over the entire surface. In addition, the shape of the 2*D* peak (Fig. 3e) obtained after the thermal treatment is characteristic of bilayer graphene, being well fitted by four Lorentzians [40,55,56]. The position of these four components coincides, within the experimental error, with values determined by Malard et al. [56] for exfoliated bilayer graphene. This shows that the original strain of −0.2% observed for the pristine sample is released due to the intercalation. Thus, the carrier density is the main factor which determines the position and shape of the G_h and G_l peaks. Based on their positions [50,54], we find that the bilayer graphene has a mean carrier density of about 1×10^{13} cm^{-2} (*p*-type), with the splitting of the *G* band indicating that the bottom and top layers are doped to different degrees. The Raman results confirm the quasi-free-standing nature of the bilayer graphene and support the XPS results. Similarly to the *G* band, the 2*D* peak shape and width do not change for measurements performed on different regions, showing that the BL decoupling leading to bilayer graphene is homogeneous over the entire sample surface. The high quality of the material is confirmed by the observation of only a very weak *D* peak (at about 1375 cm^{-1}). This peak, which is regarded to be defect-induced [57], has an intensity of <4% of the intensity of the *G* peak, as shown in the Raman mapping displayed in Fig. 4. This confirms the high-quality of the material.

In addition to the known graphene *G*, 2*D*, and *D* features, additional spectral structures are always observed in the pristine sample in the range between 1200 and 1650 cm^{-1} (Fig. 3a). However, after oxygen intercalation, these features are no longer observed in the spectrum (Fig. 3b), in a similar way to what has been reported for graphene obtained by hydrogen intercalation [20]. These additional Raman features are associated with the BL while it is still covalently bonded to

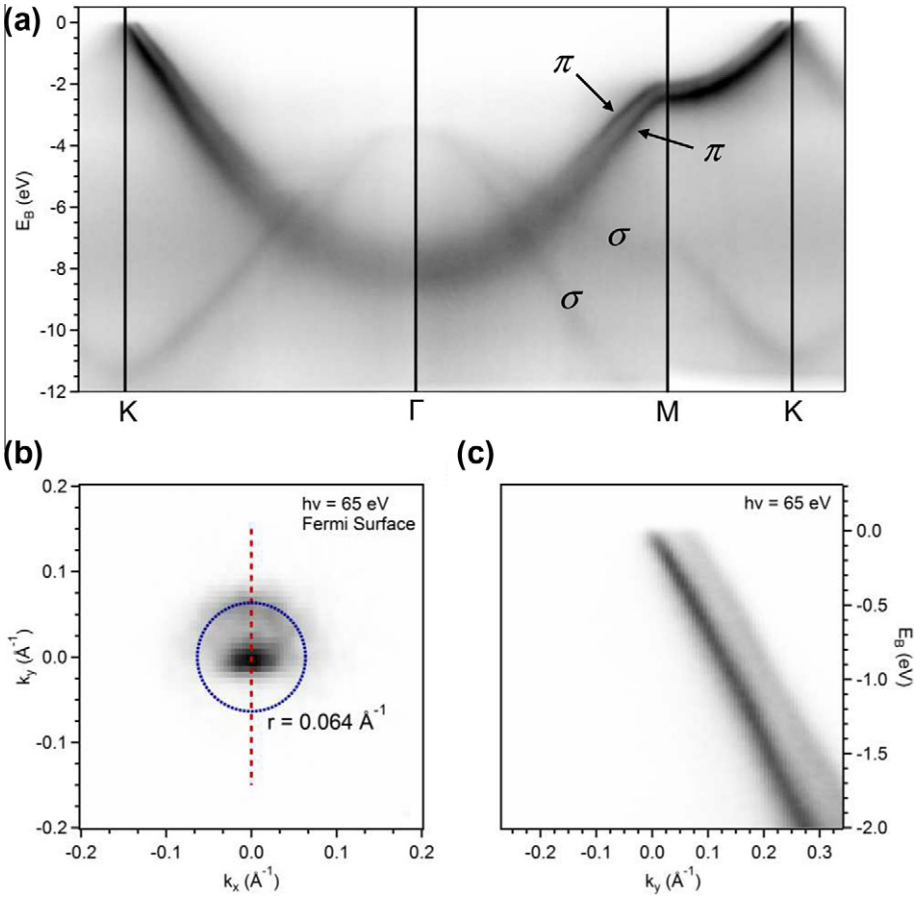

Fig. 5 – Photoelectron intensity maps for oxygen intercalated bilayer graphene. (a) Overview map *vs.* binding energy for $E_B = -12$ eV to E_F and parallel momentum for the *Γ–K*, *Γ–M* and *M–K* directions of the graphene Brillouin zone. This map clearly shows the presence of two *π*-bands and thus the existence of double layer graphene. (b) High resolution map *vs.* parallel momentum in two perpendicular directions of the Fermi surface. The dotted circle centered at the *K*-point denotes the Fermi momentum. (c) High resolution map *vs.* binding energy for $E_B = -2$ eV to E_F and parallel momentum along the dashed red line in (b), showing the linear dispersion of the *π*-bands. All spectra taken with $E_{hv} = 65$ eV, linear polarized.

SiC.[1] Interestingly, the absence of these structures provides a simple way to verify the conversion of a BL into graphene as a consequence of intercalation.

ARPES measurements (Fig. 5) also confirm the presence of bilayer graphene. In Fig. 5a the well-known graphene σ-bands are clearly resolved. The two π-bands from bilayer graphene are clearly visible around the *M*-Point as well as along the Γ–*K* direction in the vicinity of the *K*-Point. No SiC bulk bands are observed over the whole graphene Brillouin zone. In non-intercalated bilayer graphene samples, *i.e.* two layers of graphene on top of the BL, bulk bands are also not visible [24]. This confirms the high-quality and uniformity of the produced bilayer graphene. The Dirac point is not visible due to hole doping of the intercalated bilayer graphene. The amount of doping, calculated from the magnitude of the Fermi wavevector (dotted blue circle in Fig. 5b), is of 0.0068 holes per unit cell or 1.3×10^{13} cm^{-2} (in agreement with Raman results). In contrast to earlier attempts to intercalate graphene on SiC by oxygen [34,35], the graphene layer itself remains intact to a very high degree. No oxidation or defect formation, which would be indicated by a strong broadening of the photoemission lines, can be seen (see Fig. 5a and c).

Finally, it is important to mention that the same air annealing process was applied to a BL/SiC(0001) sample but did not work with the same success. For annealing temperatures ranging up to 500 °C, the conversion of the BL into graphene was observed but not without inducing defects in the structure, as verified by Raman measurements (not shown). At 600 °C, the BL was completely etched during annealing. The protecting effect that the topmost monolayer graphene provides to the BL during the thermal annealing is intriguing and is currently under further investigation. It is also worth to notice that thermally treating epitaxial graphene in a pure O_2 atmosphere also promotes graphene etching, as previously reported [34,35]. Thus, a question that arises here is whether the O_2 present in the air is indeed the precursor responsible by the BL decoupling. One plausible explanation would be that the H_2O vapor is the oxygen precursor. Nevertheless, to clarify what is the rule of each substance in the process, further experiments are required.

4. Conclusions

We have shown that the thermal annealing of epitaxial monolayer graphene in air leads to the decoupling of the BL due to oxygen intercalation, giving rise to bilayer graphene. The quasi-free-standing bilayer, which is highly *p*-doped, offers high-quality and is homogeneous over a large area. The thermal annealing in air provides a simple and easy way to produce bilayer graphene on SiC(0001) without the need of well-controlled processes requiring either high purity atmospheres or UHV thin film deposition followed by annealing, as it is used in the other approaches for decoupling graphene.

Acknowledgments

The authors would like to thank P.V. Santos for the critical reading of the manuscript; H.-P. Schönherr, M. Höricke and C. Herrmann for technical support. Work in Erlangen was supported by the ESF in the framework of the EUROGRAPHENE project GraphicRF and by the European Union through the CRP ConceptGraphene.

[1] Fromm et al. unpublished data.

REFERENCES

[1] Novoselov KS, Geim AK, Morozov SV, Jiang D, Katsnelson MI, Grigorieva IV, et al. Two-dimensional gas of massless dirac fermions in graphene. Nature 2005;438:197–200.
[2] Novoselov KS, Jiang Z, Zhang Y, Morozov SV, Stormer HL, Zeitler U, et al. Room-temperature quantum hall effect in graphene. Science 2007;315:1379.
[3] Zhang Y, Tang T-T, Girit C, Hao Z, Martin MC, Zettl A, et al. Direct observation of a widely tunable bandgap in bilayer graphene. Nature 2009;459:820–3.
[4] Novoselov KS, Geim AK, Morozov SV, Jiang D, Zhang Y, Dubonos SV, et al. Electric field effect in atomically thin carbon films. Science 2004;306:666–9.
[5] Berger C, Song Z, Li X, Wu X, Brown N, Naud C, et al. Electronic confinement and coherence in patterned epitaxial graphene. Science 2006;312:1191–6.
[6] Emtsev KV, Bostwick A, Horn K, Jobst J, Kellogg GL, Ley L, et al. Towards wafer-size graphene layers by atmospheric pressure graphitization of silicon carbide. Nat Mater 2009;8:203–7.
[7] Dimitrakopoulos C, Lin Y-M, Grill A, Farmer DB, Freitag M, Sun Y, et al. Wafer-scale epitaxial graphene growth on the Si-face of hexagonal SiC (0001) for high frequency transistors. J Vac Sci Technol B 2010;28:985–92.
[8] Lin Y-M, Dimitrakopoulos C, Jenkins KA, Farmer DB, Chiu H-Y, Grill A, et al. 100-GHz transistors from wafer-scale epitaxial graphene. Science 2010;327:662.
[9] Waldmann D, Jobst J, Speck F, Seyller Th, Krieger M, Weber HB. Bottom-gated epitaxial graphene. Nat Mater 2011;10:357–60.
[10] Hass J, Varchon F, Millán-Otoya JE, Sprinkle M, Sharma N, de Heer WA, et al. Why multilayer graphene on 4H-SiC(000−1) behaves like a single sheet of graphene. Phys Rev Lett 2008;100:125504.
[11] Hass J, Feng R, Millán-Otoya JE, Li X, Sprinkle M, First PN, et al. Structural properties of the multilayer graphene/4H-SiC(000−1) system as determined by surface X-ray diffraction. Phys Rev B 2007;75:214109.
[12] First PN, de Heer WA, Seyller Th, Berger C, Stroscio JA, Moon J-S. Epitaxial graphene on silicon carbide. MRS Bull 2010;35:296–305 [and references therein].
[13] Riedl C, Zakharov AA, Starke U. Precise in situ thickness analysis of epitaxial graphene layers on SiC(0001) using low-energy electron diffraction and angle resolved ultraviolet photoelectron spectroscopy. Appl Phys Lett 2008;93:033106.
[14] Riedl C, Starke U, Bernhardt J, Franke M, Heinz K. Structural properties of the graphene-SiC(0001) interface as a key for the preparation of homogeneous large-terrace graphene surfaces. Phys Rev B 2007;76:245406.
[15] Jobst J, Waldmann D, Speck F, Hirner R, Maude DK, Seyller Th, et al. Quantum oscillations and quantum hall effect in epitaxial graphene. Phys Rev B 2010;81:195434.
[16] Weingart S, Bock C, Kunze U, Emtsev KV, Seyller Th, Ley L. Influence of growth conditions of epitaxial graphene on the film topography and the electron transport properties. Physica E 2010;42:687–90.

[17] Emtsev KV, Speck F, Seyller Th, Ley L, Riley JD. Interaction, growth, and ordering of epitaxial graphene on SiC(0001) surfaces: a comparative photoelectron spectroscopy study. Phys Rev B 2008;77:155303.
[18] Mattausch A, Pankratov O. Ab initio study of graphene on SiC. Phys Rev Lett 2007;99:076802.
[19] Riedl C, Coletti C, Iwasaki T, Zakharov AA, Starke U. Quasi-free-standing epitaxial graphene on SiC obtained by hydrogen intercalation. Phys Rev Lett 2009;103:246804.
[20] Speck F, Jobst J, Fromm F, Ostler M, Waldmann D, Hundhausen M, et al. The quasi-free-standing nature of graphene on H-saturated SiC(0001). Appl Phys Lett 2011;99:122106.
[21] Virojanadara C, Zakharov AA, Yakimova R, Johansson LI. Buffer layer free large area bi-layer graphene on SiC (0001). Surf Sci 2010;604:L4–7.
[22] Speck F, Ostler M, Röhrl J, Jobst J, Waldmann D, Hundhausen M, et al. Quasi-freestanding graphene on SiC(0001). Mater Sci Forum 2010;629:645–8.
[23] Lee K, Kim S, Points MS, Beechem TE, Ohta T, Tutuc E. Magnetotransport properties of quasi-free-standing epitaxial graphene bilayer on SiC: evidence for bernal stacking. Nano Lett 2011;11:3624–8.
[24] Ohta T, Bostwick A, Seyller Th, Horn K, Rotenberg E. Controlling the electronic structure of bilayer graphene. Science 2006;313:951–4.
[25] Oostinga JB, Heersche HB, Liu X, Morpurgo AF, Vandersypen LMK. Gate-induced insulating state in bilayer graphene devices. Nat Mater 2008;7:151–7.
[26] Castro EV, Novoselov KS, Morozov SV, Peres NMR, Dos Santos JMBL, Nilsson J, et al. Biased bilayer graphene: semiconductor with a gap tunable by the electric field effect. Phys Rev Lett 2007;99:216802.
[27] Walter AL, Jeon K-J, Bostwick A, Speck F, Ostler M, Seyller Th, et al. Highly *p*-doped graphene obtained by fluorine intercalation. Appl Phys Lett 2011;98:184102.
[28] Wong SL, Huang H, Wang Y, Cao L, Qi D, Santoso I. Quasi-free-standing epitaxial graphene on SiC(0001) by fluorine intercalation from a molecular source. ACS Nano 2011;5:7662–8.
[29] Xia C, Watcharinyanon S, Zakharov AA, Yakimova R, Hultman L, Johansson LI, et al. Si intercalation–deintercalation of graphene on 6H-SiC(0001). Phys Rev B 2012;85:045418.
[30] Gierz I, Suzuki T, Weitz RT, Lee DS, Krauss B, Riedl C, et al. Electronic decoupling of an epitaxial graphene monolayer by gold intercalation. Phys Rev B 2010;81:235408.
[31] Premlal B, Cranney M, Vonau F, Aubel D, Casterman D, De Souza MM, et al. Surface intercalation of gold underneath a graphene monolayer on SiC(0001) studied by scanning tunneling microscopy and spectroscopy. Appl Phys Lett 2009;94:263115.
[32] Emtsev KV, Zakharov AA, Coletti C, Forti S, Starke U. Ambipolar doping in quasi-free standing epitaxial graphene on SiC(0001) controlled by Ge intercalation. Phys Rev B 2011;84:125423.
[33] Virojanadara C, Watcharinyanon S, Zakharov AA, Johansson LI. Epitaxial graphene on 6H-SiC and Li intercalation. Phys Rev B 2010;82:205402.
[34] Oida S, McFeely FR, Hannon JB, Tromp RM, Copel M, Chen Z, et al. Decoupling graphene from SiC(0001) via oxidation. Phys Rev B 2010;82:041411(R).
[35] Ostler M, Koch RJ, Speck F, Fromm F, Vita H, Hundhausen M, et al. Decoupling the graphene buffer layer from SiC(0001) via interface oxidation. Mater Sci Forum 2012;717–720:649–52.
[36] Oliveira Jr MH, Schumann T, Ramsteiner M, Lopes JMJ, Riechert H. Influence of the silicon carbide surface morphology on the epitaxial graphene formation. Appl Phys Lett 2011;99:111901.
[37] Seyller Th, Emtsev KV, Gao K, Speck F, Ley L, Tadich A, et al. Structural and electronic properties of graphite layers grown on SiC(0001). Surf Sci 2006;600:3906–11.
[38] Tanaka S, Morita K, Hibino H. Anisotropic layer-by-layer growth of graphene on vicinal SiC(0001) surfaces. Phys Rev B 2010;81:041406(R).
[39] Tuinstra F, Koenig JL. Raman spectrum of graphite. J Chem Phys 1970;53:1126–30.
[40] Ferrari AC, Meyer JC, Scardaci V, Casiraghi C, Lazzeri M, Mauri F, et al. Raman spectrum of graphene and graphene layers. Phys Rev Lett 2006;97:187401.
[41] Thomsen C, Reich S. Double resonant Raman scattering in graphite. Phys Rev Lett 2000;85:5214–7.
[42] Mohiuddin TMG, Lombardo A, Nair RR, Bonetti A, Savini G, Jalil R, et al. Uniaxial strain in graphene by Raman spectroscopy: *G* peak splitting, gruneisen parameters, and sample orientation. Phys Rev B 2009;79:205433.
[43] Huang M, Yan H, Heinz TF, Hone J. Probing strain-induced electronic structure change in graphene by Raman spectroscopy. Nano Lett 2010;10:4074–9.
[44] Pisana S, Lazzeri M, Casiraghi C, Novoselov KS, Geim AK, Ferrari AC, et al. Breakdown of the adiabatic Born–Oppenheimer approximation in graphene. Nat Mater 2007;6:198–201.
[45] Das A, Pisana S, Chakraborty B, Piscanec S, Saha SK, Waghmare UV, et al. Monitoring dopants by Raman scattering in an electrochemically top-gated graphene transistor. Nat Nanotechnol 2008;3:210–5.
[46] Schmidt DA, Ohta T, Beechem TE. Strain and charge carrier coupling in epitaxial graphene. Phys Rev B 2011;84:235422.
[47] Robinson JA, Puls CP, Staley NE, Stitt JP, Fanton MA, Emtsev KV, et al. Raman topography and strain uniformity of large-area epitaxial graphene. Nano Lett 2009;9:964–8.
[48] Zabel J, Nair RR, Ott A, Georgiou T, Geim AK, Novoselov KS, et al. Raman spectroscopy of graphene and bilayer under biaxial strain: bubbles and balloons. Nano Lett 2012;12:617–21.
[49] Malard LM, Elias DC, Alves ES, Pimenta MA. Observation of distinct electron–phonon couplings in gated bilayer graphene. Phys Rev Lett 2008;101:257401.
[50] Yan J, Villarson T, Henriksen EA, Kim P, Pinczuk A. Optical phonon mixing in bilayer graphene with a broken inversion symmetry. Phys Rev B 2009;80:241417(R).
[51] Bruna M, Borini S. Observation of Raman *G*-band splitting in top-doped few-layer graphene. Phys Rev B 2010;81:125421.
[52] Mak KF, Lui CH, Shan J, Heinz TF. Observation of an electric-field-induced band gap in bilayer graphene by infrared spectroscopy. Phys Rev Lett 2009;102:256405.
[53] Gava P, Lazzeri M, Saitta AM, Mauri F. Probing the electrostatic environment of bilayer graphene using Raman spectra. Phys Rev B 2009;80:155422.
[54] Mafra DL, Gava P, Malard LM, Borges RS, Silva GG, Leon JA, et al. Characterizing intrinsic charges in top gated bilayer graphene device by Raman spectroscopy. Carbon 2012;50:3435–9.
[55] Graf D, Molitor F, Ensslin K, Stampfer C, Jungen A, Hierold C, et al. Spatially resolved Raman spectroscopy of single- and few-layer graphene. Nano Lett 2007;7:238–42.
[56] Malard LM, Nilsson J, Elias DC, Brant JC, Plentz F, Alves ES, et al. Probing the electronic structure of bilayer graphene by Raman scattering. Phys Rev B 2007;76:201401(R).
[57] Ferrari AC. Raman spectroscopy of graphene and graphite: disorder, electron–phonon coupling, doping and nonadiabatic effects. Solid State Commun 2007;143:47–57.